Structure Under Mount Rainier, Washington, Inferred From Teleseismic Body Waves

CHARLES A. LANGSTON

Department of Geosciences, Pennsylvania State University, University Park, Pennsylvania 16802

Teleseismic long-period *P* waves recorded at the World-Wide Standard Seismograph Network station LON (Longmire, Washington) are shown to exhibit strong anomalous particle motion not attributable to instrument miscalibration or malfunction. In particular, a large and azimuthally smoothly varying tangential component is observed after vector rotation of horizontal *P* waves into the ray direction and after application of a deconvolution technique which equalizes effective source time functions and removes the instrument response. These tangential waves attain amplitudes comparable to the radial component and demonstrate wave form antisymmetry about a NNE azimuth. A model which contains a single high-contrast interface dipping toward the NNE at a depth of 15–20 km can explain most of the characteristics of the long-period *P* wave data, provided dips are greater than about 10° and only the interference of *P* and *Ps* generated at the interface is considered. The model breaks down for later arrivals which are presumably multiples or scattered waves. Examination of long-period *S* waves from several deep teleseisms shows a prominent *Sp* arrival 18 s before *S*. The timing of this phase conversion suggests an interface at about 145-km depth, and its sense of polarity suggests that the velocity contrast is from higher to lower velocities as depth decreases. This interface may correspond to the bottom of the upper mantle low-velocity zone in the area.

INTRODUCTION

From a geologist's point of view, the top of the earth's crust is composed of a myriad of differing rock types with readily discernable lateral variations in lithologies and structures. On the basis of these surface observations it is easy and probably justified to assume that the entire crustal and upper mantle column behaves in a similar complicated way. Recent high-resolution reflection profiling and other seismological studies are beginning to support this view [e.g., *Smithson*, 1978; *Aki et al.*, 1977]. However, when seismic waves are used to deduce earth structure, the usual state of affairs is to assume vertically inhomogeneous earth models with no lateral variations. This assumption is good in many cases because, to first order, the earth appears to be radially stratified and seismic waves fortunately average over distance scales comparable to their wavelength.

This paper examines an interesting case where the seismic data cannot be explained with any vertically inhomogeneous nonlaterally varying earth model. Teleseismic *P* and *S* waves as recorded at the World-Wide Standard Seismograph Network (WWSSN) station LON (Longmire, Washington) were examined to determine crustal and upper mantle structure beneath the station. A previous study of teleseismic body waves at COR (Corvallis, Oregon) and of *P* wave forms recorded teleseismically from the 1965 Puget Sound earthquake indicated that the area of western Washington and Oregon might be underlain by a distinct low-velocity zone (LVZ) [*Langston*, 1977*a*; *Langston and Blum*, 1977]. The base of this LVZ was inferred to be at 55-km depth under Puget Sound and at 45-km depth under COR. LON, which is located on the flank of Mount Rainier, a Quaternary stratovolcano, was chosen for study in an attempt to define the limits of this LVZ.

It was immediately apparent upon examination and comparison of the long-period *P* wave form data that earth structure at LON is radically different from structure under COR. As is the usual case when new data are considered, new questions and problems immediately arose with respect to both the regional structure picture and seismic wave propagation. The most dramatic aspect of the data from LON is that long-period *P* waves exhibited a large tangential component of ground motion. The simple existence of 'tangential *P* waves' automatically precludes any explanation or interpretations using honogeneous plane layered earth models, since the *P-SV* and *SH* wave systems are decoupled.

The study of these waves will be based on a timid extension of standard seismological practice. Using theory presented in a previous paper [*Langston*, 1977*b*], earth models will still have planar interfaces, but these interfaces will be allowed to dip. A three-dimensional ray-tracing formalism is used to find the path of rays in the structure. Ray amplitudes are computed by first decomposing the incident ray into *P-SV* and *SH* components in local interface coordinates, multiplying each amplitude by the appropriate plane wave reflection or transmission coefficient, and then propagating the wave to the next interface, where the procedure is repeated. Diffracted waves from structure edges or corners are not included. Hence all 'tangential *P*' wave effects will be explained by off-azimuth arrivals of primary, converted, and reverberated rays. This is a hypothesis which was only partially successful in explaining the observed *P* wave data, whether because of a breakdown in theory (existence of diffracted waves) or in assuming planar interfaces (other geometries or topography).

After a short description of regional tectonics and setting, this study will be presented in four parts. First, the long-period *P* wave form data recorded at LON will be presented with a discussion of instrument calibration. This is crucial, since instrument miscalibration or malfunction is the first likely cause of apparent tangential *P* waves. Next, a general method for equalizing the wave form data for arbitrary effective source time function will be discussed. Afterward, the equalized *P* wave form data will be interpreted by calculating theoretical ray amplitudes and synthetic seismograms from earth models with planar dipping interfaces. The final section presents results concerning long-period *S* wave form data. While not adding significant constraints to earth models deduced from the *P* wave data, there is an indication of an interface at approximately 145-km depth under LON from *Sp* precursor observations.

Paper number 9B0335.
0148-0227/79/009B-0335$01.00

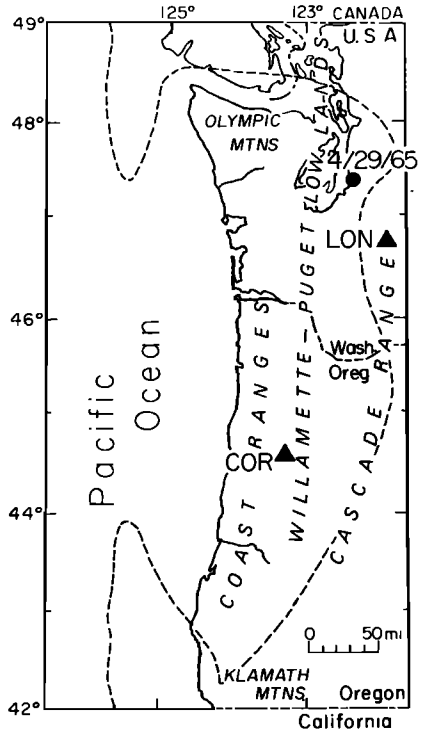

Fig. 1. Index map of the Pacific Northwest region. Triangles indicate locations of the WWSSN stations COR (Corvallis, Oregon) and LON (Longmire, Washington). Also shown is the location of the 1965 Puget Sound earthquake and major physiographic provinces of the area. The dashed line represents the inferred limit of a Tertiary eugeosyncline [after *Snavely and Wagner*, 1963].

Regional Setting

Longmire station is located on the south flank of Mount Rainier, which is the highest member of the Cascade Range of northern California, Oregon, and Washington (Figure 1). Mount Rainier is a relatively young feature with vulcanism initiating in early Pleistocene and continuing into recent times [*Fiske et al.*, 1963]. In the plate tectonics scheme the Cascades are part of a continental arc of andesitic vulcanism related to subduction of oceanic lithosphere from Cape Mendecino, California, to Vancouver Island, British Columbia. An oceanic ridge system consisting of the Gorda and Juan De Fuca rises is located a few hundred kilometers offshore. The small Gorda–Juan De Fuca plate, lying between the continent and the oceanic ridge system, is the last remnant of the previously more extensive Farallon plate which was subducting under western North America throughout the Tertiary [*Atwater*, 1970]. For a more comprehensive summary of tectonics in the Pacific Northwest, please refer to *Riddihough* [1978] or *Langston and Blum* [1977].

Geophysical studies in the Mount Rainier area have usually been of a reconnaissance nature. Gross crustal structure is essentially unknown; the station LON is almost always used as the last station of long-range refraction profiles [*Johnson and Couch*, 1970; *Berg et al.*, 1966; *Zuercher*, 1975]. However, their studies and others [e.g., *Dehlinger et al.*, 1965] indicate that the Cascades are a region of crustal transition between higher mantle *P* velocities and thicker crustal sections to the east compared to low *Pn* velocities and thin crust to the west. Studies of teleseismic *P* wave residuals indicate that LON is not a particularly anomalous station, at least for average teleseismic travel times (for example, see *Sengupta and Julian* [1976] for a synopsis). However, *Lin* [1974] suggested that the relative travel time residual of LON with respect to the rest of the University of Washington Puget Sound array was consistent with an eastward dipping high wave velocity slab or an eastward thinning low-velocity zone.

Microearthquakes have been monitored in the Mount Rainier area on an intermittent basis using a small portable array [*Unger and Decker*, 1970; *Unger and Mills*, 1972]. An upper crustal *P* velocity of 6.1 km/s was determined using a well-timed blast recorded on this array. This relatively high velocity is consistent with propagation through the Tatoosh pluton, which is thought to directly underlie the volcano [*Fiske et al.*, 1963]. Gravity results indicate that this pluton may only be a few kilometers thick (Z. F. Daneš, personal communication, 1978).

Because there are few data to control average crustal properties, this study will necessarily be limited to determining types of structures consistent with the data. Therefore it will represent further reconnaissance on the nature of crustal structure under Mount Rainier.

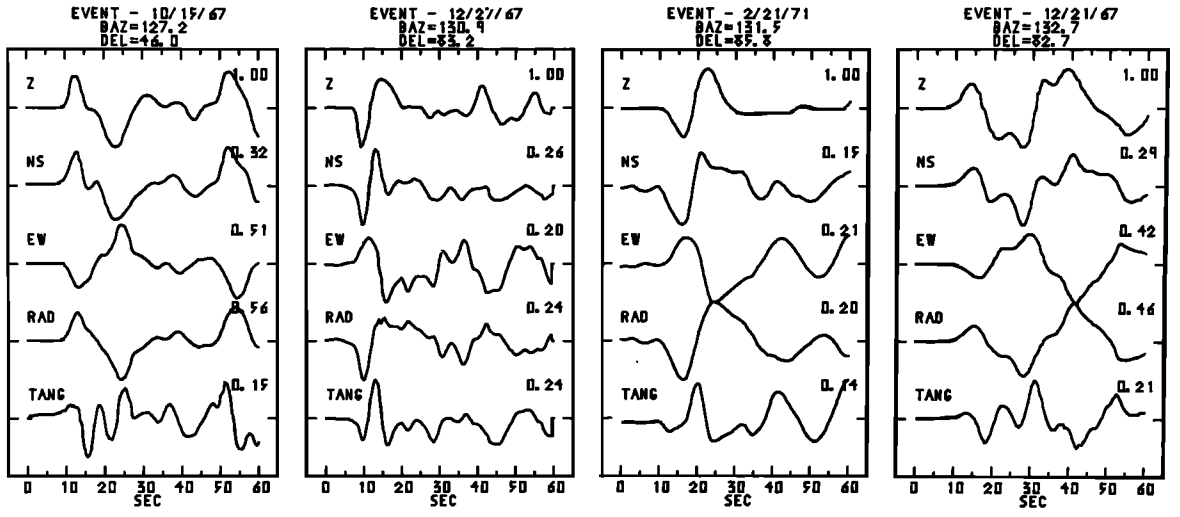

Fig. 2*a*. Display of *P* wave form digitized data and vector rotations into the theoretical ray back azimuth. Positive vertical, radial, and tangential ground motion is defined as up, away from the source, and clockwise around the source (looking downward), respectively. Note the relatively large tangential components. Events on October 15, 1967; December 27, 1967; February 21, 1971; and December 21, 1967.

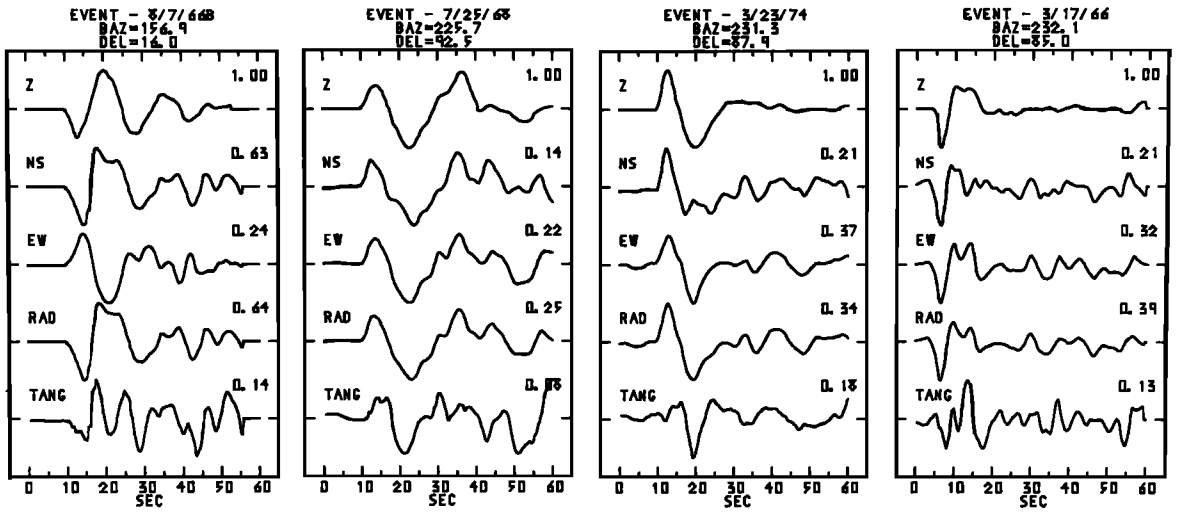

Fig. 2*b*. Same scheme as Figure 2*a* for events on August 7, 1966 B; July 25, 1968; March 23, 1974; and March 17, 1966.

LONG-PERIOD *P* WAVE FORM DATA AND INSTRUMENT CALIBRATION

Figure 2 shows vector rotations of *P* waves from 12 events distributed in three quadrants of back azimuth. Back azimuth is defined as azimuth clockwise from north, to the source as seen from the receiver. Source parameters were obtained from ISC (International Seismological Center) and PDE (Preliminary Determinations of Epicenters) bulletins and are listed in Table 1 for all events used in this study. Initially, data from only a few deep teleseismic events were examined in the hope of observing *P* to *S* converted phases on the radial component. By modeling the time and amplitude of these converted *P* waves in the time domain, estimates of crustal thickness and interface velocity contrasts may be obtained. See *Burdick and Langston* [1977] for further details on this kind of time domain interpretation. Once it became apparent that vector rotation of the horizontal *P* wave forms into the theoretical ray direction yielded significant tangential motion for one back azimuth, more azimuthal coverage was needed to determine the nature of the probable nonhorizontal structure. Teleseisms were obtained to cover as many back azimuths as possible to apply dipping interface theory following a suggestion made by the author in a previous work [*Langston*, 1977*b*]. Although the other three quadrants were covered, no events were obtained with northwest back azimuths (Figure 2).

The vertical and horizontal component *P* wave data of Figure 2 were digitized at an equal time increment of 0.25 s from paper copies made from film chips. The top and bottom of each trace was digitized and then averaged together. Several events were chosen for each quadrant to serve as a consistency check on the digitizing and rotation procedure.

A few pertinent observations can be made about the *P* waves of Figure 2. The first obvious one is that each rotation yielded a significant tangential component approximately one third to one half as large as the radial component. In all cases it is considerably above the seismic noise level. We must first determine if this is a real effect. Several possibilities concerning the origin of the tangential component come to mind other than earth structure: source mislocation (wrong back azimuth), digitizing error, and instrument calibration are some. Source mislocation can be ruled out, since the error required would be thousands of kilometers. In any case, even if the wrong back azimuth was used, both horizontal components should differ only by an amplitude factor and be identical in wave shape, provided structure is horizontal. A simple com-

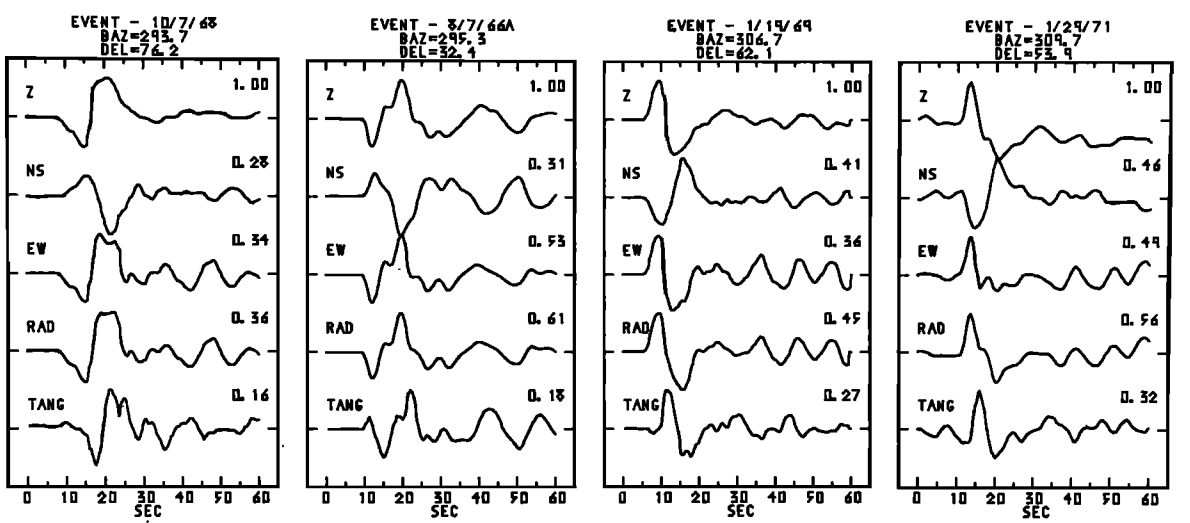

Fig. 2*c*. Same scheme as Figure 2*a* for events on October 7, 1968; August 7, 1966 A; January 19, 1969; and January 29, 1971.

TABLE 1. Event Parameters

Date	Time, UT	Position, deg	M	H, km	Location	Distance, deg	Back Azimuth, deg
March 17, 1966	1550:32.3	21.08°S, 179.15°W	5.9	627	Tonga	85.0	232.1
Aug. 7, 1966 A	0213:04.3	50.57°N, 171.22°W	6.3	29	Aleutians	32.4	295.3
Aug. 7, 1966 B	1736:28.5	31.74°N, 114.51°W	5.7	32	Gulf of California	16.0	156.9
Oct. 15, 1967	0800:52.6	11.92°N, 85.98°N	6.2	181	Nicaragua	46.0	127.2
Dec. 21, 1967	0225:21.0	21.89°S, 70.07°W	6.0	20	Chile	82.7	132.7
Dec. 27, 1967	0917:50.3	21.29°S, 68.20°W	6.3	91	Chile	83.2	130.9
July 25, 1968	0723:02.0	30.97°S, 178.13°W	6.5	17	Kermadec	92.5	225.7
Oct. 7, 1968	1920:20.8	26.29°N, 140.70°E	6.1	518	Bonin Islands	76.2	293.6
Jan. 19, 1969	0702:07.9	44.89°N, 143.21°E	6.3	238	Hokkaido	62.1	306.7
Jan. 29, 1971	2158:03.2	51.69°N, 150.97°E	6.0	515	Sea of Okhotsk	53.9	309.7
Feb. 21, 1971	1035:19.7	23.81°S, 67.20°W	6.0	166	Chile-Argentina	85.8	131.5
March 6, 1972	1850:16.8	50.14°N, 148.80°E	5.4	569	Sea of Okhotsk	55.9	309.0
March 23, 1974	1428:35.4	23.9°S, 179.8°E	6.1	535	Fiji	87.9	231.3

parison of any of the NS-EW components in Figure 2 shows that there are always major differences in wave shapes. Major digitizing error was ruled out from comparison of the digitized traces with the original data. Some error undoubtedly does occur, which is why many events were examined. Consistency of equalized wave shapes of events from the same azimuth is good, indicating little numerical error. This will be presented in a later section.

Instrument miscalibration is the most serious factor which must be considered. *Mitchell and Landisman* [1969] indicate that calibration of the long-period WWSSN system may be off by as much as 20% in the free periods and damping of the seismometer and galvanometer. Experience with calibration of a similar long-period system at Pasadena has also indicated possible calibration errors of up to 20% (F. Lehner, personal communication, 1977). A parameter study was made where seismograph constants were varied by 20%. Resulting theoretical instrument responses [*Hagiwara,* 1958] were convolved with a simple pulse similar, for example, to the duration of the December 12, 1967, event. Differences in wave shapes were slight and did not approach any of the characteristics of the data. Figure 3 shows calibration pulses for the long-period system at LON taken from the records containing the October 7, 1968, event. The calibration current and electromechanical constant for each component is given in Table 2. Aside from a small amount of long-period drift on the EW component the shapes and amplitudes of the pulses are similar. A check on the relative amplitudes expected between components based on the data of Table 2 yields only a 3% difference from observed amplitudes. Therefore the LON long-period system was reasonably calibrated.

One more powerful argument can be made against the instrument system being grossly miscalibrated. Figure 4 shows a comparison of wave forms for two events with similar pulselike wave forms on the vertical component. The difference in back azimuth is almost 180°. Now, if one horizontal component was grossly in error so that it, say, produced an obviously longer pulse than the other component, then it should behave in a similar fashion for all recorded events. For example, let us say that the EW component seen for the December 27, 1967, event of Figure 4 consistently produces a long-duration pulse as compared to the NS component. However, the January 29, 1971, event data look reversed. In this case the NS component is obviously of longer duration compared to the EW component. Therefore the assumption that instruments are consistently miscalibrated is erroneous, which leads to the conclusion that earth structure is causing the effect.

P WAVE EQUALIZATION PROCEDURE

Shallow teleseisms and teleseisms with complicated apparent source functions had to be used to provide good azimuthal coverage. Deep events with simple pulselike wave forms on the vertical component are preferred because later *P* to *S* conversions on the horizontal components may then be investigated directly [*Burdick and Langston,* 1977]. Even when such data are available, however, there still remain differences between effective source time functions, which can cause significant differences in synthetic seismogram calculations [e.g., *Langston,* 1977*a*]. Thus a way of equalizing the data to compensate for differing source time functions would be helpful. A method of doing this is suggested by the form of the data and theoretical considerations.

In the time domain the form of the theoretical displacement response for a *P* plane wave impinging under a stack of horizontal or dipping interfaces can be given by

$$\begin{aligned} D_V(t) &= I(t) * S(t) * E_V(t) \\ D_R(t) &= I(t) * S(t) * E_R(t) \\ D_T(t) &= I(t) * S(t) * E_T(t) \end{aligned} \tag{1}$$

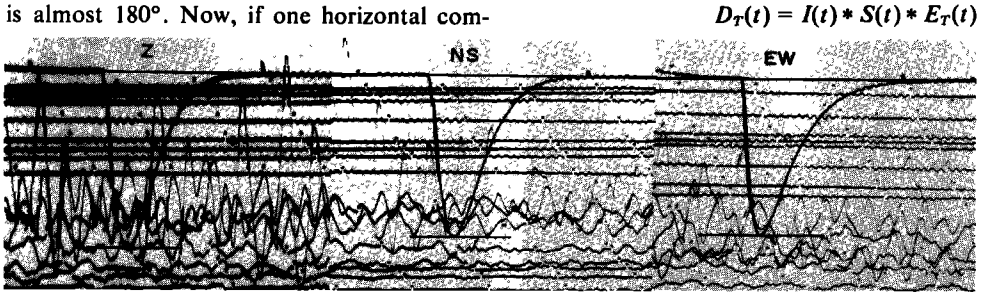

Fig. 3. Long-period calibration pulses taken from the October 7, 1968, recordings. Refer to Table 2 for calibration constants.

TABLE 2. Calibration Constants for the October 7, 1968, Calibration Curves

Component	Calibration Current, mA	Electromechanical Constant, N/A
Z	0.2	0.106
NS	0.2	0.099
EW	0.2	0.097

where $S(t)$ is the effective source time function of the impinging wave, $I(t)$ is the instrument impulse response, and the $E_V(t)$, $E_R(t)$, and $E_T(t)$ are the vertical, radial, and tangential structure impulse responses, respectively. $S(t)$ may be quite complicated and related to dislocation time history and source area reverberations, for example. The $E(t)$ are of the form

$$E(t) = \sum_{i=1}^{n} \{\alpha_i \delta(t - \tau_i) + \beta_i H[\delta(t - \tau_i)]\} \tag{2}$$

where α_i and β_i are constants related to the product of reflection-transmission coefficients, $\delta(t)$ is the Dirac delta function, τ_i is the travel time of the ith ray, and $H[\ ]$ represents the Hilbert transform operator. The summation is done over n rays. A common way to calculate the $E(t)$ for plane layered models is to use a propagator matrix technique in the frequency domain [*Haskell*, 1960, 1962]. In this case, for phase velocity greater than any P or S velocity in the earth model, β_i is zero for all i, n is infinity, and $E_T(t)$ does not apply. Equations (1) also do not apply, in general, to the case of an incident S wave. Even in the horizontally plane layered case, $S(t)$ for SV waves will often be different from that of the SH wave.

A common observation made from teleseismic data of simple deep events is that the vertical component of ground motion behaves as a pulselike time function convolved with the instrument response with only minor later arrivals [*Burdick and Helmberger*, 1974]. Theoretical calculations for typical crustal structures show that crustal reverberations and converted phases on the vertical component of steeply incident P waves are minor even if a high-contrast interface is allowed to dip [*Burdick and Langston*, 1977; *Langston*, 1977*b*]. However, this starts to break down for extremely high velocity contrasts (> 2 km/s). Thus we can approximate $S(t)$ by letting

$$I(t) * S(t) \simeq D_V(t) \tag{3}$$

The implicit assumption is that $D_V(t)$ behaves mostly like one Dirac delta function. Assuming that instrument responses are matched between components, $E_R(t)$ and $E_T(t)$ may be found by deconvolving $I(t) * S(t)$ from $D_R(t)$ and $D_T(t)$. In the frequency domain this process is given by

$$E_R(\omega) = \frac{D_R(\omega)}{I(\omega)S(\omega)} \simeq \frac{D_R(\omega)}{D_V(\omega)}$$
$$E_T(\omega) = \frac{D_T(\omega)}{I(\omega)S(\omega)} \simeq \frac{D_T(\omega)}{D_V(\omega)} \tag{4}$$

$E_R(\omega)$ and $E_T(\omega)$ are then retransformed back into the time domain. Note the similarity of this technique with the spectral ratio method previously used in these kinds of studies [e.g., *Kurita*, 1973]. The important difference is that phase information is conserved. Furthermore, the resulting time series may be interpreted directly as a seismogram, allowing times and amplitudes of arrivals to be examined in a relatively unambiguous manner.

Assuming, for the moment, no noise, an estimate of the error in assuming (3) can be explicitly examined. From ray calculations in a layer over a half-space model, the largest arrival on the vertical component besides direct P is the first P reverberation. Consider therefore

$$E_V(t) = \alpha_1 \delta(t - \tau_1) + \alpha_2 \delta(t - \tau_2) \tag{5}$$

where the first term on the right is direct P and the other is reverberated P. It can be shown, to first order, that the inerse operation of $E_V(t)$, $E_V^{-1}(t)$, is given by

$$E_V^{-1}(t) = \frac{1}{\alpha_1}\delta(t + \tau_1) - \frac{\alpha_2}{\alpha_1^2}\delta(t + 2\tau_1 - \tau_2) + O\left(\frac{\alpha_2^2}{\alpha_1^2}\right) \tag{6}$$

where

$$E_V(t) * E_V^{-1}(t) = \delta(t)$$

For simplicity, let $\alpha_1 = 1$ and $\tau_1 = 0$. In practice, $\alpha_2/\alpha_1 \sim -0.1$. Therefore there will be no deconvolution error in applying $E_V^{-1}(t)$ or $1/E_V(\omega)$ to (4) until relative times equal to τ_2. Since α_2/α_1 is smaller than relative amplitudes of converted phases on the horizontal component, the error is small even for later times.

Unfortunately, the deconvolution procedure of (4) is numerically unstable because signals are band-limited and contain random noise. In practice, a technique suggested by *Helmberger and Wiggins* [1971] and *Dey-Sarkar and Wiggins* [1976*b*] is used to estimate the deconvolution. This estimate is then multiplied by the transform of a Gaussian to limit the final frequency band by excluding high-frequency signals not obviously present in the original recordings. In the frequency domain this process is given by

$$E_R'(\omega) = \frac{D_R(\omega)\bar{D}_V(\omega)}{\Phi_{SS}(\omega)} \cdot G(\omega) \tag{7}$$

where

$$\Phi_{SS}(\omega) = \max\{D_V(\omega)\bar{D}_V(\omega),\ c \max [D_V(\omega)\bar{D}_V(\omega)]\}$$

and

$$G(\omega) = e^{-\omega^2/4a^2}$$

$E_R'(\omega)$ is the deconvolved 'radial earth response,' and the bar over $D_V(\omega)$ denotes the complex conjugate. The function $\Phi_{SS}(\omega)$ can be thought of as simply being the autocorrelation

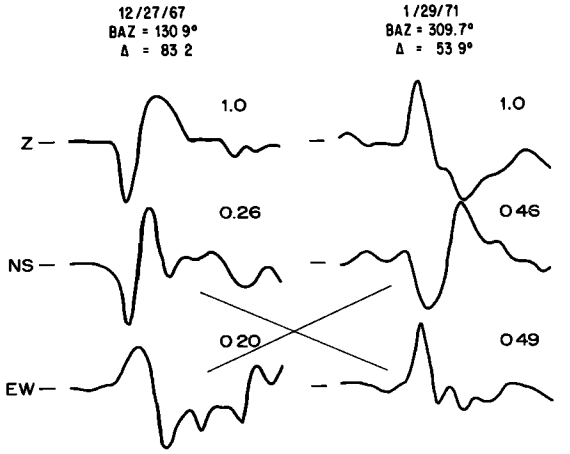

Fig. 4. Comparison of P wave form data from two events with opposing back azimuths. Note that pulse character alternates for each horizontal component, indicating that the effect is from earth structure and not instrument miscalibration.

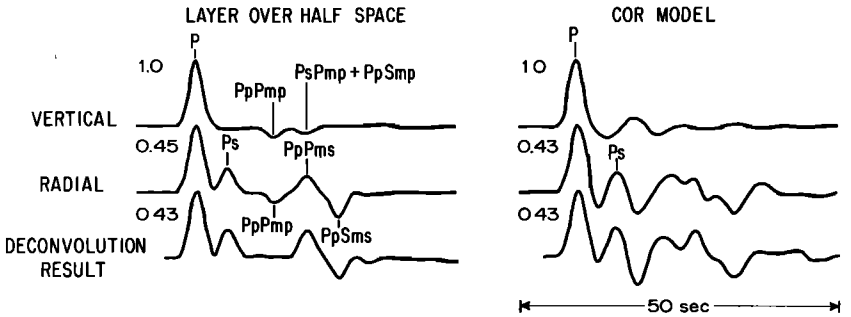

Fig. 5. Test of deconvolution technique with synthetic data using two plane layered earth models (Table 3). A Gaussian effective time history has been convolved with the vertical and radial displacement for each model. The two bottom curves show the result of the deconvolution procedure in which an instrument operator and a simple pulselike time function were included in the synthetic data. Phase nomenclature is after *Båth and Stefánsson* [1966].

of $D_V(\omega)$ with any spectral troughs filled to a level depending on the parameter c. In every deconvolution to be presented, $c = 0.01$, and a, the parameter controlling the width of the Gaussian, was set to 0.7. A Gaussian was chosen for its smooth symmetric shape and pulselike character in the time domain. The width of the Gaussian was chosen to approximately match observed pulse widths of the simpler vertical wave forms. This helps to insure against getting too much detail which is not warranted by the observations.

Figure 5 shows synthetic examples of the deconvolution process. A layer-over-half-space and the COR model (Table 3) were chosen to test the assumptions inherent in (4) and (7). Synthetics were calculated using *Haskell*'s [1962] method. In each case the vertical component shows significant *P* multiples later in the wave train. The deconvolution result was obtained using (7) for synthetic wave forms which included convolutions of the instrument and an effective time function comparable to the December 27, 1967, event (Figure 2). Careful comparison of the synthetic radial response and the deconvolution result shows that wave shape differences are small and consist primarily of removing arrivals which end up as *P* waves at the receiver. Note, for example, the absence of the first *P* reverberation, *PpPmp*, in the layer-over-half-space model. This will be true in general for any plane layered structure under which incident waves have small angles of incidence. This occurs, since converted *S* waves are almost exclusively found on the horizontal components; the amplitude ratios of rays which are *P* waves in their last ray segments, in relation to the direct wave, will be the same on both components. Therefore this deconvolution technique (and any other spectral ratio technique) essentially removes *P* waves, except for the direct arrival, and leaves conversions and reverberations of the *P* to *S* type for the plane layered problem. This will not be strictly true for the dipping interface problem, since each ray can have a different angle of incidence and

TABLE 3. Earth Models

Layer	*Vp*, km/s	*Vs*, km/s	ρ, g/cm³	*Th*, km
		Layer Over Half Space		
1	6.0	3.5	2.6	40.0
2	8.1	4.7	3.2	...
		COR Model		
1	5.5	3.0	2.6	10.0
2	6.7	3.9	2.8	6.0
3	8.0	4.6	3.2	5.0
4	7.9	4.5	3.15	1.5
5	7.8	4.2	3.1	2.0
6	7.7	3.7	3.0	1.5
7	7.5	3.5	2.95	1.5
8	7.2	3.3	2.9	2.0
9	6.9	3.3	2.85	2.5
10	6.6	3.3	2.85	12.9
11	8.0	4.6	3.2	...
		LON Model		
1	6.0	3.0	2.7	20.0
2	8.0	4.6	3.2	70.0
3	7.8	4.0	3.2	35.0
4	8.1	4.65	3.2	...

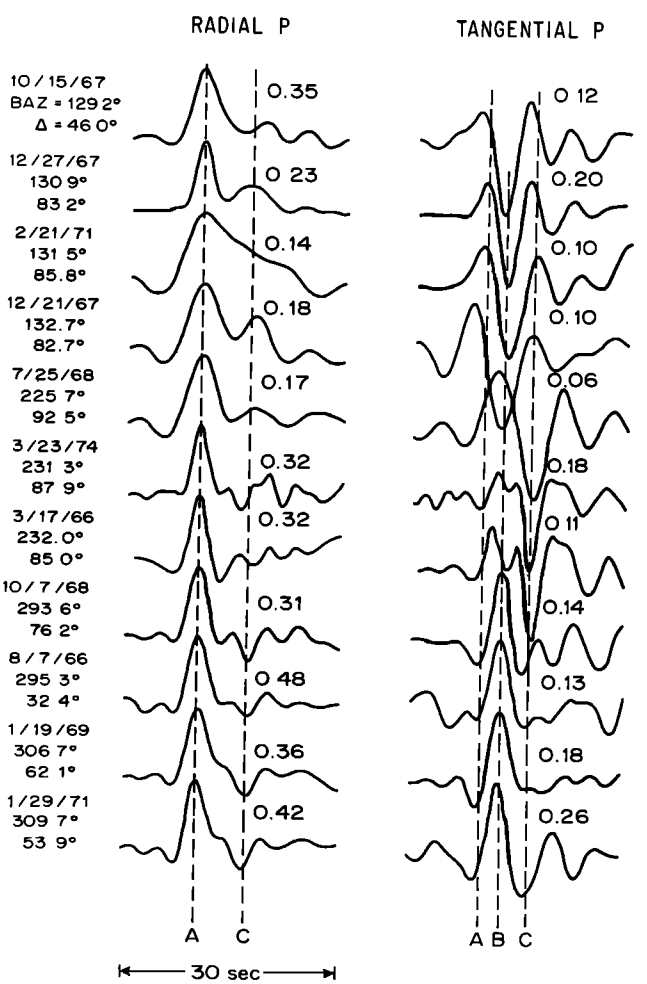

Fig. 6. Deconvolution of effective time functions and instrument operators of the radial and tangential *P* wave forms in Figure 2. The dashed lines indicate interpretations of arrivals. Amplitudes, relative to the vertical component, are shown by each time series.

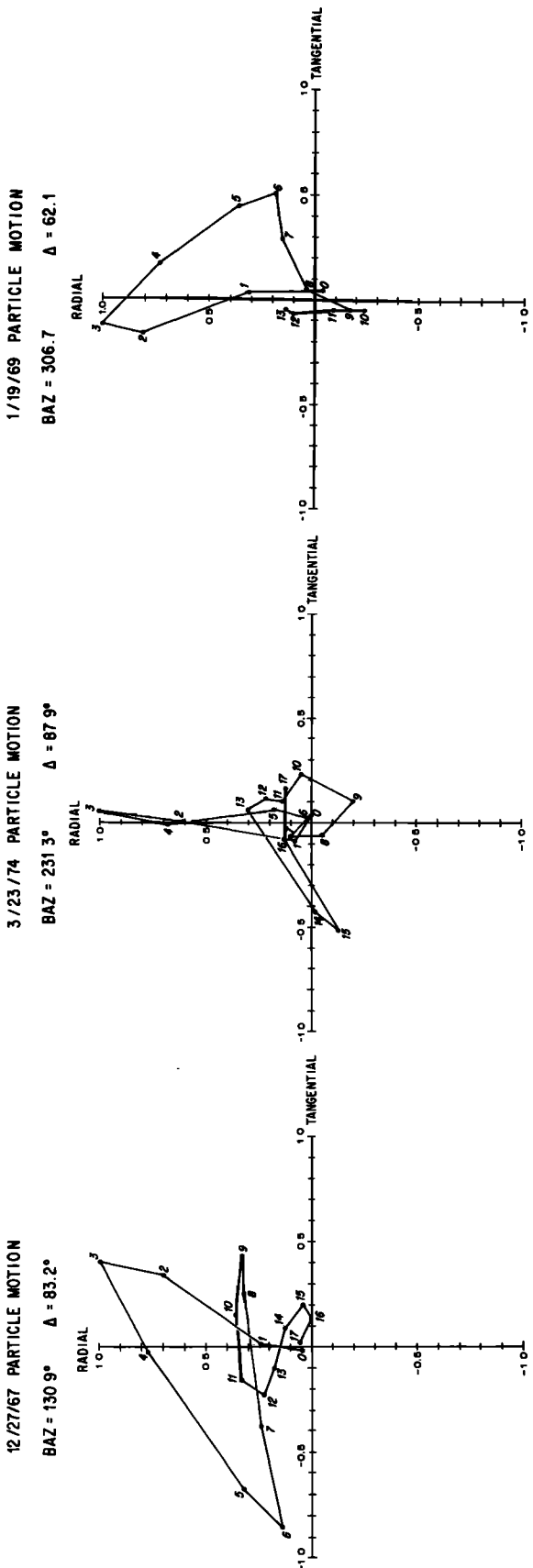

Fig. 7. Radial-tangential particle motion plots for three deconvolved events shown in Figure 6. A time increment of 1 s is used with time numbered sequentially on the plots. In all cases the radial maximum at 3 s corresponds to the peak time of direct *P* (arrival A).

azimuth of arrival, ruining the relative amplitude similarity of *P* waves between vertical and radial components.

The radial and tangential *P* wave forms of Figure 2 were deconvolved using this technique and are shown in Figure 6. A 5-s cosine taper was applied to the ends of each time series before deconvolution. Although the wave shape details of waves from similar back azimuths can vary, there is good consistency in overall shape and timing. Spurious arrivals before direct *P* are caused from a combination of original seismic noise and the filling of troughs in the autocorrelation function of the vertical component. In other words, the original effective source time function coupled with noise can still cause some effect through the deconvolution procedure. The stability of tangential and radial wave shapes for events of similar back azimuth over time, along with previous arguments, shows that particle motion effects are due to earth structure and not instrument problems.

The peak times of three prominent arrivals are shown by the dashed lines of Figure 6. Arrival A is the peak of the direct *P* wave. On the tangential components it is seen to be small and interfering with arrival B. Arrival B is predominant in the southeast and northwest quadrants; note also the general wave form antisymmetry about northeast-southwest azimuths. Arrival C is represented primarily by the tangential *P* wave forms of southwest back azimuths. It also seems to occur in the radial *P* wave forms as a positive peak at the top of Figure 6 changing to a negative arrival near the bottom. Figure 7 shows normalized radial-tangential particle motion for the three representative wave form groups of Figure 6. These plots demonstrate the off-azimuth arrival of direct *P* and the large tangential secondary arrivals.

Interpretation of the *P* Wave Forms

We are now faced with the rather formidable task of explaining the wave forms of Figure 6. Ideally, the goal is to make a physical model of earth structure under LON whose wave response matches the observed wave forms. However, the inverse problem is ill posed because there are few outside constraints on crustal properties, the crust is likely to be laterally heterogeneous from geologic observations, and the data are a result of nearly vertical propagation of body waves even though the events are azimuthally distributed. This kind of data can only resolve velocity contrasts and average crustal travel times. Because of these problems and keeping Ocham's Razor in mind, a hypothesis-testing approach will be taken by examining the effects of simple planar dipping earth models.

We start (and end) with a single dipping interface model. Calculations of responses for such models indicate that tangential *P* wave components are azimuthally antisymmetric about an azimuth perpendicular to the strike of the interface [*Langston*, 1977*b*]. The polarities of tangential *P* and the *Ps* conversion at the interface indicate the direction of dip. Figure 8 shows a plot of arrival B polarity versus back azimuth. From its reverse polarity compared to direct tangential *P*, its relative arrival time of 3 s, and its azimuthal symmetry characteristics, arrival B is interpreted to be a *Ps* conversion occurring at an interface from 15 to 20 km in depth, depending on crustal velocities. Assuming, for the moment, that the velocity contrast is from higher to lower velocity as depth decreases, the allowable dip azimuth lies within the northern sector bounded by solid lines on Figure 8. Note that polarity information was taken from the August 7, 1966 B event (BAZ = 156.9°). The deconvolution of this event was poor as determined from presignal noise in the final result. This was probably partly due

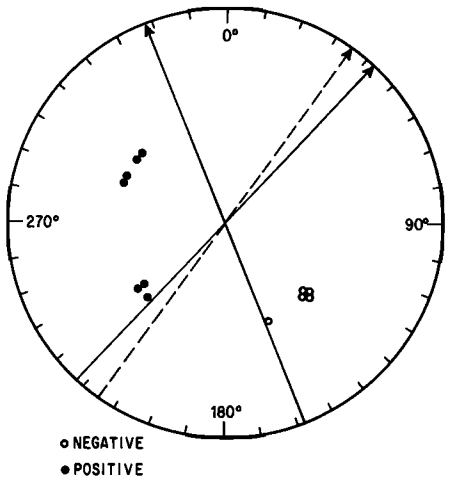

Fig. 8. Polar plot of *Ps* tangential polarity versus back azimuth. There is no significance in the radius length to each point. Positive tangential polarity is taken to be clockwise, looking downward around the source. Direct tangential *P* wave polarity is opposite for each datum. Acceptable interface dip directions are located in the northern sector bounded by the two solid arrows. The dotted arrow indicates dip direction based on symmetry of NW and SE wave forms.

to digitizing problems, since the vertical component was high amplitude, but also partly due to the event's short range. Many different phases with differing phase velocities are undoubtably present in these data, invalidating the assumption of one incident angle for the incident wave. The dashed line (Figure 8) is dip azimuth for the interface inferred from symmetry consideration. The SE and NW groups are more mirror symmetric than are the SE and SW wave groups; hence, and on the basis of model calculations, it is more reasonable without other constraining data to locate the SE and NW groups at similar azimuthal positions relative to dip azimuth. Note that wave antisymmetry, off-azimuth *P* arrivals, and high tangential wave amplitude all argue against anisotropic medium effects as discussed by *Keith and Crampin* [1977].

Although polarities can indicate interface dip and strike, wave amplitudes must be used to determine interface velocity contrast and dip magnitude. The radial and tangential wave forms of Figure 6 exhibit large variation in amplitudes relative to the vertical component. Part of this variation is due to differing incident angles, but probably the greater part is due to numerical digitization and rotation error. To get an estimate of interface contrast and dip and also to see the trade-offs involved, a numerical search and test inversion procedure was set up to model inferred *P* and *Ps* tangential relative amplitudes. Amplitudes were read from four distributed events (December 27, 1967; July 25, 1968; October 7, 1968; and January 19, 1969) and were assigned 70% standard errors. This large error conservatively incorporates the factor of 2 variation seen in the relative amplitude data. Crustal velocities and densities for the upper layer and interface strike were assumed with interface dip and velocity contrast being incrementally varied. *P* and *Ps* amplitudes were calculated for each model and compared to the observations. Those falling within the allowable 70% were deemed successes, and those outside failures. If all four datums were satisfied by some structure model, then that model was considered viable and was output from the program.

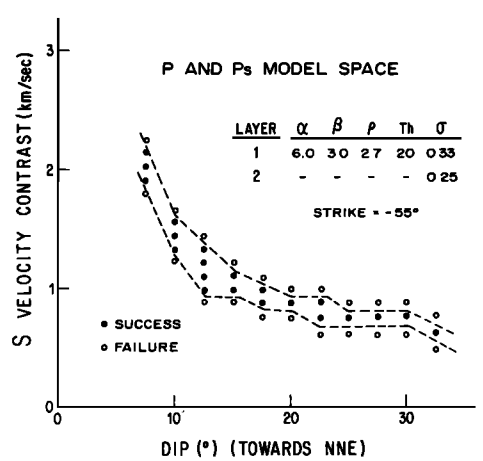

Fig. 9. Inversion result to determine bounds of interface dip and *S* velocity contrast which explain tangential *P* and *Ps* relative amplitudes assuming a 70% standard error. See text for details.

Figure 9 shows the result from one such inversion. The choice of upper crustal velocities is not very crucial to the location of the boundaries of the model space for *P* and *Ps* amplitudes, although a high Poisson ratio helps the *P*/*Ps* ratio. Lower *P* and *S* velocities would tend to raise the boundaries, preserving the important general characteristics. Changing interface strike within the bounds of Figure 8 also does little to these results. First note that there is a pronounced trade-off between interface velocity contrast and dip; high contrasts require small dips, and vice versa. Also note that any successful model requires large contrasts and large dips to approximate observed amplitudes. Thus the causative structure can be considered a major tectonic feature of the area.

By symmetry in the problem and considering the behavior of the transmission coefficients at the interface, it is logical to assume that similar results could be obtained for an interface

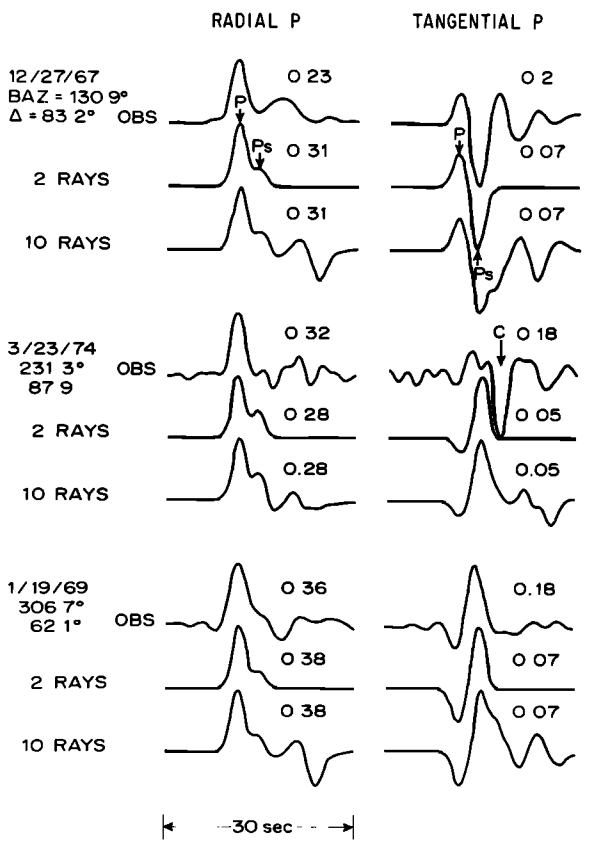

Fig. 10. Comparison of deconvolved radial and tangential *P* waves with synthetics calculated for the single dipping interface model.

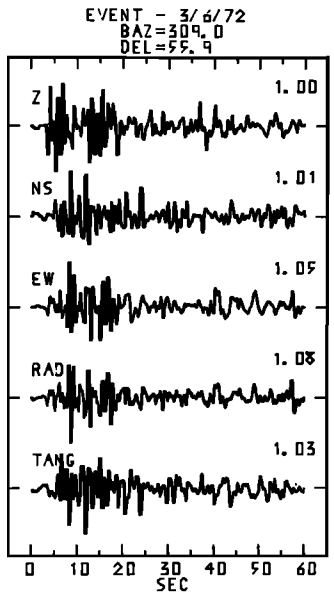

Fig. 11. Vector rotation of short-period P wave data. Note larger overall amplitude of horizontal components relative to the vertical.

dipping in the opposite direction with the opposite velocity contrast. However, when this kind of low-velocity zone model was tested, no model could be found to explain the observed amplitude. Angles of incidence of waves in low-velocity zone models were much less than those occurring with the previous normal contrast models; i.e., incident horizontal ray parameter (phase velocity) was the same. Hence induced ray azimuth anomalies and surface incident angles were smaller, reducing tangential amplitudes.

Figure 10 displays synthetic seismogram comparisons with the observed for the three best deconvolved events. These were chosen on the basis of low presignal noise and representation of their respective back azimuth groups. The crustal model of Figure 9 was used with an S velocity contrast and dip of 1.08 km/s and 12.5°, respectively. Two calculations are shown for each observation. In the first, only the rays P and Ps were included. The other calculation includes eight other important multiples and converted reverberations in the single dipping interface model. These rays produce the secondary oscillations seen after Ps in the 10-ray model. The purpose in showing these two calculations is to demonstrate both the partial success and obvious limitations of naively assuming the single dipping interface model. First note how well polarities and wave shapes are explained with inclusion of only P and Ps in the model. This is true even of the March 23, 1974, event if the large observed downswing (arrival C) is ignored for the moment. Inclusion of the other conversions and reverberations do little to help matters, however. Although the size of the reverberations approximate the observed for December 27, 1967, they do little to explain arrival C for March 23, 1974. Some insight into the physics of these rays provides an excuse, if not an explanation, for why the model breaks down so quickly. Azimuth anomalies for P and Ps refracting through the interface are of the order of 10°–20°. That is, their apparent azimuths of arrival are off by this amount with respect to true back azimuth. Rays which reverberate even once in the structure may have very large azimuth anomalies approaching 90° or more, depending on the phase conversion sequence. Thus coherent arrival of these multiples depends on the interface being planar for large horizontal distances, since typical ray paths follow a tortuous route through the structure to the receiver. If we assume that arrival C is an off-azimuth reverberation by this argument, then the structure is obviously not planar over the distances required. Arrival C could also represent a diffraction effect from unmodeled topography or other discontinuous structure. There have been previous observations of large secondary arrivals associated with body wave–to–surface wave conversion at topographic discontinuities from analysis of array data [*Key*, 1967]. However, without $dT/d\Delta$ and azimuth information for these later arrivals, not much more can be said about them.

Further insight and anxiety can be obtained by examining the effect of LON structure on short-period P waves. Figure 11 is an example of a P wave vector rotation of an event from the Sea of Okhotsh recorded at Longmire. First note that both the radial and tangential components attain larger overall amplitudes than the vertical component. Assuming that the first 3 s of the wave forms represents the direct P wave (as inferred from the long-period observations), the radial-vertical ampli-

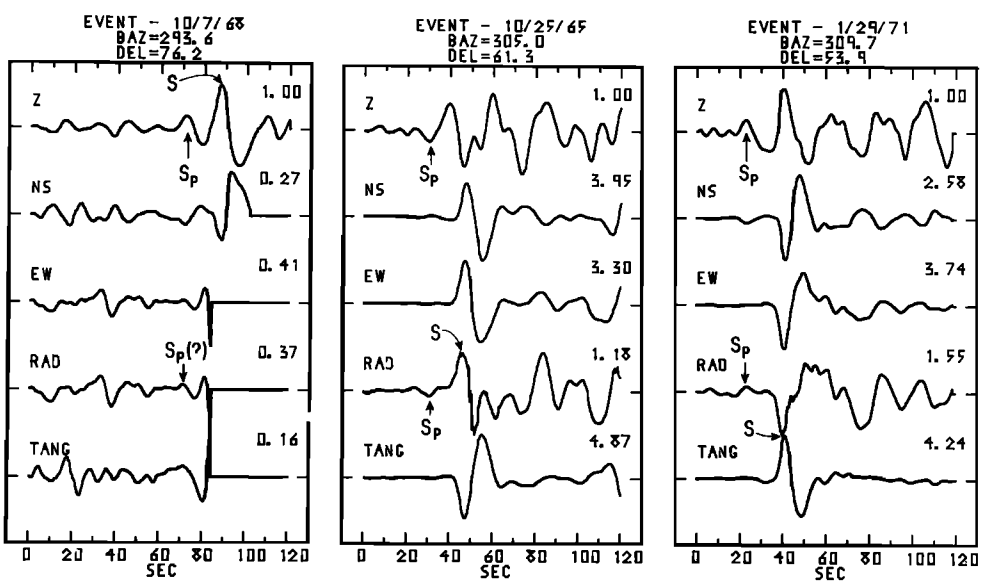

Fig. 12. Vector rotation of S wave data from three deep events. Interpretations of S and Sp phases are shown. The EW component of the October 7, 1968, event is truncated because the trace was off scale.

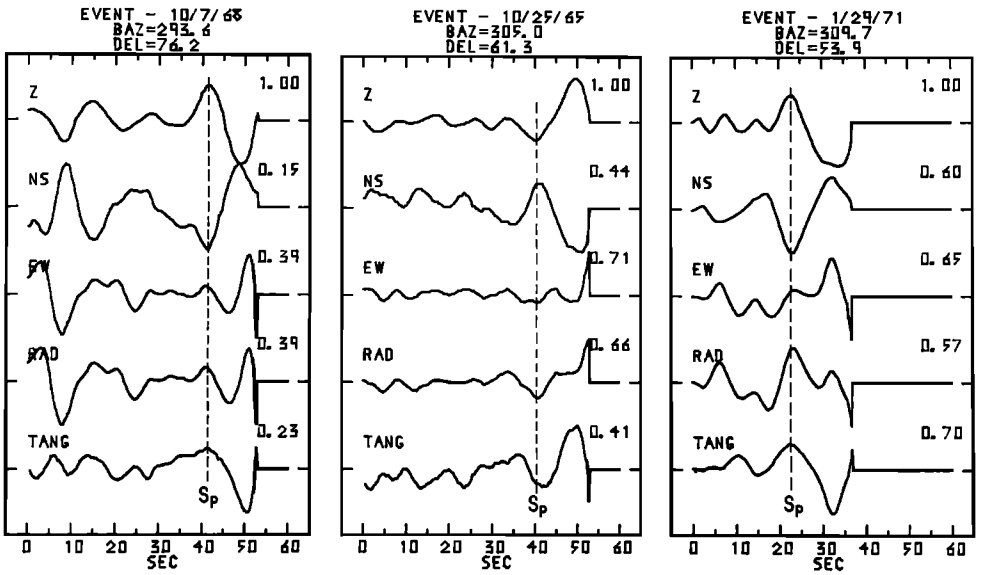

Fig. 13. Seismogram detail of the portion before direct S for the three events of Figure 12.

tude ratio does seem normal for the angle of incidence involved. However, if the large-amplitude arrival 3–4 s after direct P on the radial component is the short-period equivalent of arrival B, the long-period Ps conversion, then it implies extreme frequency dependence not supplied by the single planar dipping interface model. No such amplitude ratio is seen for long-period radial P waves from any back azimuth (Figure 6). A possible mechanism for this effect could be frequency-dependent geometric spreading effects caused by undulations on the interface, provided the wavelength of these possible undulations are of the order of the wavelength of short-period waves. Long-period waves could be expected to average over these possible undulations. SH ray calculations in severe basin type structures indicate that internal caustics and focusing can produce large secondary arrivals [*Hong and Helmberger*, 1978].

In any case it is plain that there remain many problems in explaining even some of the first-order effects observed in the wave form data. What is important is the compelling evidence that there exists a major laterally heterogeneous structure under LON capable of severely distorting long-period seismic waves. To a fair approximation, part of this structure includes a high-contrast dipping interface, approximately planar, at lower crustal depths.

Long-Period S Wave Forms and Sp Conversions

Long-period S wave forms from several deep events were investigated with the hope of finding Sp conversions to determine more constraints on the dipping interface model suggested by the P wave form data. S wave form data are necessarily limited to those of simple deep events in the distance range 45°–85°. P to S and S to P near-source conversions produce complicated effective source functions for shallow source SV waves masking the effects of near-receiver conversions. S-coupled P_L wave distortion for distances less than 45° and core phases for distances greater than about 85° further complicate interpretation. It is also desirable to obtain S data from several events to determine the stability of any Sp precursor observation [*Burdick and Langston*, 1977].

S data from three events which meet these criteria are displayed in Figure 12. Because of LON's particular position with respect to zones of deep earthquakes, satisfactory data are limited to events occurring in the northwest Pacific. Of particular interest in Figure 12 is the prominent Sp precursor with an

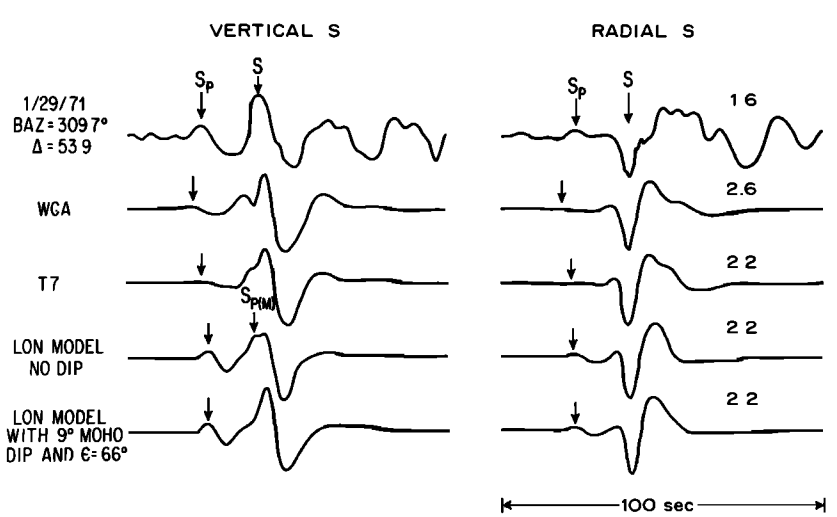

Fig. 14. Comparison of observed and synthetic S waves for the January 29, 1971, event. See text for details.

18-s lead time before direct *S*. This phase is of the same polarity as direct *S* on the vertical component but is of opposite polarity on the radial component. It is also largest on the vertical component, which is consistent with its *P* wave interpretation. The relative polarity and timing of this *Sp* phase suggest conversion at an interface at about 145-km depth with a velocity contrast from higher to lower velocities as depth decreases.

Figure 13 shows rotations of the same data up to the arrival of direct *S*. Although there is some noise at this level on the tangential component, *Sp* does seem to have tangential particle motion. This observation is consistent in polarity with an *Sp* to *S* conversion at the dipping structure seen by the *P* waves. It may also be due in part to dip on the 145-km-depth interface.

Interpretation of the relative amplitudes of *Sp* to *S* is rather difficult because there is poorer azimuthal and effective source time function control. If the tangential *SH* wave is any indication of *SV* effective time function, then Figure 12 suggests fairly simple pulselike incident waves. However, if the conversion is dipping, there could be large azimuthal variation in the *Sp/S* amplitude ratio, and hence data from other azimuths are needed to exclude this possibility. Nevertheless, some fruitful insight may be gained by examining a few model calculations.

Figure 14 displays four different model studies of the January 29, 1971, event data. WCA is an upper mantle model derived from short-period *P* wave form data, appropriate to the LON area, by *Dey-Sarkar and Wiggins* [1976*a*]. Model T7 was derived from short-period and long-period *P* wave form data by *Burdick and Helmberger* [1978] and is appropriate for the western United States. *S* wave velocities were derived from these *P* wave models by assuming a Poisson solid ($\sigma = 0.25$). The responses to WCA and T7 were calculated using *Haskell*'s [1962] method for plane layered structures. Note from Figure 14 that an *Sp* arrival is produced from conversion at the lower boundary of the upper mantle low-velocity zone which has approximately the correct time advance, relative to *S*, but severely underestimates the observed *Sp/S* ratio. The large *Sp* arrival several seconds before *S* in both WCA and T7 calculations is the conversion from the Moho.

In the absence of dip, larger *Sp/S* amplitude ratios may be obtained by increasing the *S* velocity contrast across the interface [*Jordan and Frazer*, 1975]. This is demonstrated in Figure 14 by the LON model with no dipping interfaces (Table 3). This model is, of course, very idealized; it is only presented to show the type of contrasts needed to explain the *Sp/S* amplitude ratio. Crustal structure in the LON model is limited to a single layer 20 km thick. Note that although the amplitude of the *Sp* conversion from the base of the LVZ is approximately correct, the *Sp* conversion from the crust-mantle interface at 20 km is apparently much too large. However, the effects of the dipping interface inferred from the *P* wave form data have not been included in these models. If the same velocity contrast at this crust-mantle interface is assumed, a dip of 9° may be determined from Figure 9, which explains the *P* and *Ps* tangential amplitudes. *S* wave polarization angle must also be estimated, since responses from dipping structures depend on local tangential and radial coordinates at each interface [*Langston*, 1977*b*]. The polarization angle change induced in *S* waves from simple dipping interface models is of the order of the magnitude of the dip, depending on back azimuth. Therefore an estimate of polarization angle may be obtained directly from the data. From model studies, variations of approximately 15° in polarization do not cause significant wave form variations in calculated vertical and radial components unless the incident wave is nearly pure *SH* in the horizontal frame.

The bottom model in Figure 14 includes the same velocity structure as the plane layered LON model except that the Moho is allowed to dip 9° toward the northeast (strike equals −55°). A polarization angle of 66°, appropriate for the January 29, 1971, event, was also assumed. Note that the combined effects of interface dip and *S* polarization significantly reduce the *Sp*(*m*) arrival.

Besides interface contrast, interface dip toward the northwest can increase the Sp/S ratio for S waves from northwest back azimuths. Thus there is some ambiguity in assigning physical significance to the velocity contrast given in the LON model. The most important pieces of information are the relative timing and polarity of the *Sp* phase.

DISCUSSION

Like any other geophysical or geological study, this study suffers from nonuniqueness problems because of theory limitations and structure complexity. However, it is surprising in many respects that so much general information can be deduced from teleseismic data recorded at only one receiving station. Further constraints on details of the dipping structure under LON could be obtained by a logical extension of the techniques used here. A small broadband seismic array could add important $dT/d\Delta$ and azimuth of arrival information [e.g., *Havskov and Kanasewich*, 1978]. These data, coupled with ray arrival time and amplitude, would lend themselves to greater control over structure geometry, or at least provide explanations for the behavior of the data.

The results of this study also suggest that useful reconnaissance of structure at specific areas could be obtained with the temporary installation of only one well-calibrated, broadband, three-component seismic station. This would be important in aiding either earth structure studies or site selection for a permanent seismic station. In the later case the absence of large secondary and/or off-azimuth arrivals would form positive criteria for choosing the site.

The deconvolution technique for removing the effects of instrument and time function seems to be a useful way of manipulating and equalizing wave form data for these kinds of problems. The effects of numerical error and time series truncation can be estimated more easily than in spectral interpretations, since phase information is implicitly included in the deconvolved time series. For example, noncausal or presignal arrivals above the original seismic noise level are an immediate indicator of the quality of the deconvolution. Error in the assumption that the vertical *P* component consists of only the direct wave is small for most any horizontally layered structure and simple dipping structures. In these cases, if the vertical component has sizable secondary *P* arrivals, then the horizontal components have even larger amplitude converted *P* to *S* phases in relation to horizontal *P*. If, in a particular study, it is deemed that more resolution is justified by the data than is supplied by this assumption, it becomes a simple matter to calculate synthetic time series of transfer function ratios which can be compared with the data wave forms.

The tectonic and geologic implication of a high-contrast dipping interface under Mount Rainier is not clear. Because long-period waves are strongly affected by this structure it is likely that it has lateral dimensions exceeding typical long-period wavelengths of approximately 60 km or so. The 3-s relative arrival time between inferred *Ps* and *P* arrivals sug-

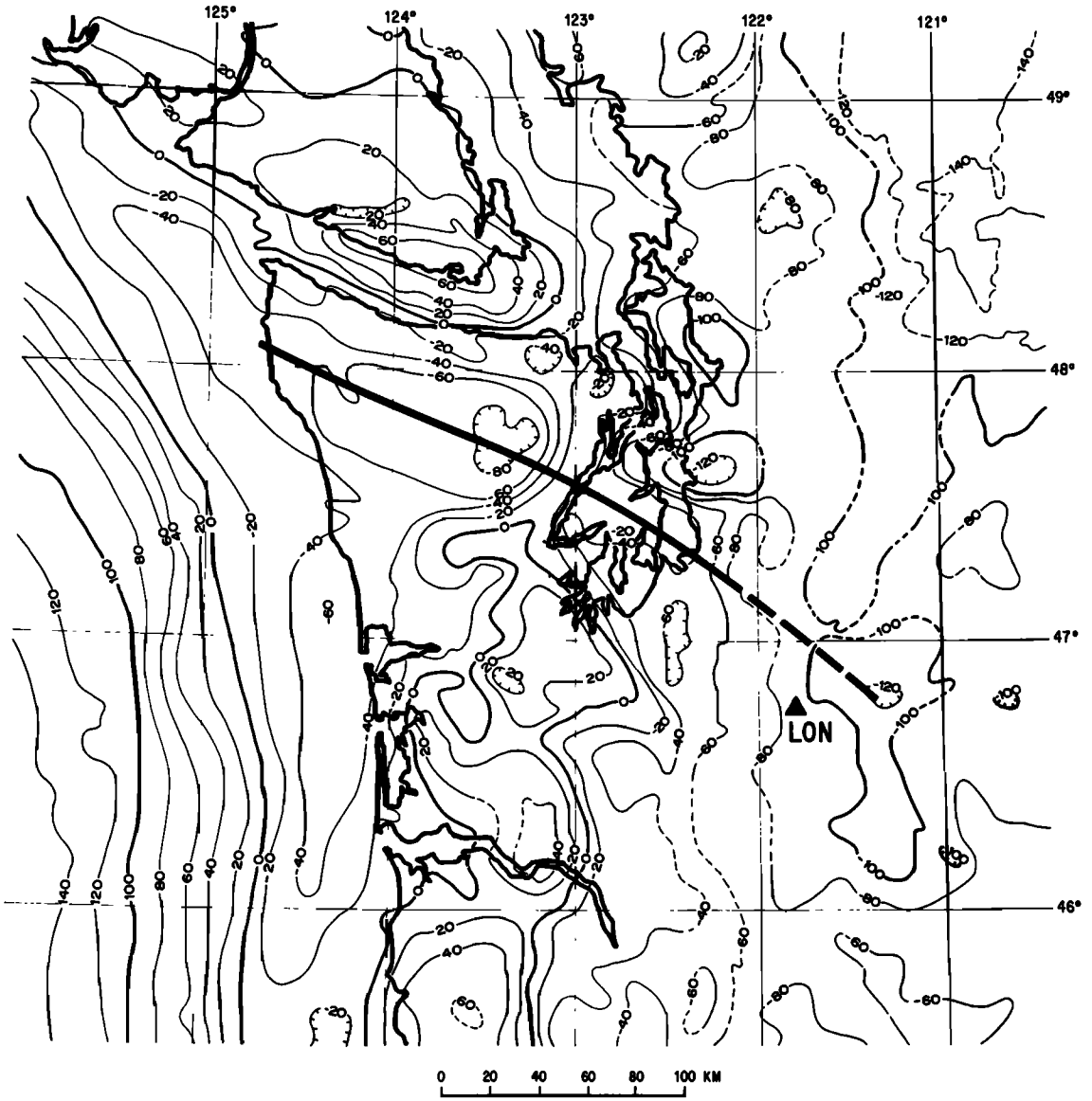

Fig. 15. Simplified Bouguer gravity anomaly map of western Washington showing tectonic trend of the Olympic Mountains and Puget Sound horst structure.

gests an interface depth of 15–20 km. The interpretation favored here is that this interface represents the Moho under Mount Rainier. From a travel time study of *P* waves from mine blasts in the southern Puget Sound area, *Zuercher* [1975] suggested that Moho depths just to the west of Mount Rainier and south of Puget Sound are only 18 or 19 km. These shallow depths are similar to a 16-km Moho depth obtained in the coast ranges of Oregon and Washington by *Berg et al.* [1966]. Zuercher's study also suggested that the Puget Sound area and environs are regions of great crustal variability with major undulations and dips on the Moho. Other geophysical studies suggest that crustal structure for the area is discontinuous and complex [e.g., *Daneš et al.*, 1965]. Thus the laterally heterogeneous structure inferred from this study is no real surprise and is consistent in character with area structure.

Figure 15 shows a simplified Bouguer gravity anomaly map for western Washington [*Bonini et al.*, 1974]. A line has been drawn to indicate the transverse tectonic trend of the Olympic Mountains and Puget Sound basement horst structure [*Daneš et al.*, 1965]. Most physiographic and tectonic trends in the Pacific Northwest are usually aligned in a north-south fashion (e.g., see Figure 1). It is interesting to note that Mount Rainier lies on the eastward extension of this transverse trend and that the trend azimuth is consistent with interface strike inferred from the *P* wave form data. Thus the Mount Rainier area may be genetically linked with structure to the west but with a complicated volcanic overprint.

Alternatively, the anomalous crustal structure may be associated with processes involving vulcanism or pluton emplacement. *LaFehr* [1965] interpreted gravity anomalies over several South Cascade volcanoes and inferred relatively large low-density aureoles under them. Although apparently masked by an upper crustal pluton under Mount Rainier (Z. F. Daneš, personal communication, 1978), this kind of lenslike structure may exist there at midcrustal depth and be responsible for the observed dipping structure. In any case, since some long-period effects were not explained by the single dipping interface model, it is very likely that the presence of Mount Rainier and its associated structures has an important effect on local wave propagation.

The most straightforward interpretation of the long-period *Sp* observations is that they are produced by conversion at the

base of the upper mantle LVZ. It is also apparent that radially symmetric earth models appropriate for the area do not explain the magnitude of the effect. This seems to imply that either structure is not radially symmetric or that there are some resolution problems with the body wave techniques employed. This assumes, of course, that the observed *Sp* amplitudes are not a fortuitous result of effective source time interference for all three events.

One purpose in looking for *Sp* arrivals was to determine if there is any evidence for a dipping slab under the Cascades [*McKenzie and Julian*, 1971; *Lin*, 1974] following suggestions made by *Sacks and Snoke* [1977] and *Snoke et al.* [1977]. However, other than the *Sp* arrival from 145-km depth, there does not seem to be any other evidence for interfaces between 145-km and 20-km depth. The relatively shallow LVZ structures inferred from COR receiver data and teleseismic wave forms from the 1965 Puget Sound earthquake do not seem to have an analogue beneath LON.

SUMMARY

Wave forms from a suite of azimuthally distributed teleseismic earthquakes were vectorially rotated into theoretical ray directions based on published epicentral parameters. Because a mixture of deep and shallow events was used, an equalization procedure was developed to remove the effect of differing source time functions and the instrument response. This method consisted of deconvolving the vertical *P* wave component from the radial and applying a Gaussian filter. It was shown that errors from including possible *P* wave multiples on the vertical component in the deconvolution algorithm were small. Large *P* multiples generally imply larger *P* to *S* conversions and reverberations in planar structures.

Equalized *P* wave forms showed good consistency for events from the same back azimuth. In particular, the tangential *P* wave forms exhibited relatively large amplitudes of one-third to one-half the radial component. These tangential wave forms were also antisymmetric about a NNE-NE azimuth. It has been shown through a series of arguments that the anomalous tangential *P* wave particle motion observed from the teleseismic observations cannot be attributed to instrument malfunction or miscalibration.

Most wave forms were sufficiently modeled by the interference of direct *P* and a *Ps* conversion from an interface at 15- to 20-km depth dipping toward the NNE. An inversion study of the polarity and amplitude of tangential *P* and *Ps* indicated that major trade-offs occur between interface velocity contrast and dip. The single dipping interface model broke down when reverberations in the structure were considered. Teleseismic short-period *P* observations also suggested that the structure wave response is frequency dependent. Thus the single dipping interface model can be considered a first approximation to the shallower structure under LON.

On the basis of nearby refraction profiles and tectonic trends it is suggested that the interface is the Moho under Mount Rainier and that the area is intimately connected with Puget Sound and Olympic Mountains structure.

S wave form data from three teleseisms were used in an attempt to constrain interface parameters inferred from the *P* data. No constraints were found on shallow structure, but an *Sp* precursor was observed with an 18-s lead time before direct *S*. Using average upper mantle and crustal velocities, the timing suggested conversion at about 145-km depth. The polarity was consistent with a normal velocity contrast from higher to lower velocities as depth decreases. Comparison of synthetic seismograms calculated from earth models appropriate for the area showed that the arrival is probably due to conversion at the base of the upper mantle LVZ. However, higher *S* velocity contrasts or dip on this interface is needed to explain the relatively large observed amplitude of *Sp*.

Acknowledgments. I would like to thank Z. F. Daneš of the University of Puget Sound for sending me a preprint of his gravity results for Mount Rainier and Doug Baumgardt for reviewing the manuscript. This research was supported by the Advanced Research Projects Agency of the Department of Defense and was monitored by the Air Force Office of Scientific Research under grant AFOSR-78-3528.

REFERENCES

Aki, K., A. Christoffersson, and E. S. Husebye, Determination of the three-dimensional seismic structure of the lithosphere, *J. Geophys. Res., 82,* 277–296, 1977.

Atwater, T., Implications of plate tectonics for the Cenzoic tectonic evolution of western North America, *Geol. Soc. Amer. Bull., 81,* 3513–3536, 1970.

Båth, M., and R. Stefánsson, *S-P* conversion at the base of the crust, *Ann. Geofis., 19,* 119–130, 1966.

Berg, J. W., Jr., L. Trembly, P. A. Emilia, J. R. Hutt, J. M. Kling, L. T. Long, W. R. McKinight, S. K. Sarmah, R. Souders, J. V. Thiruvathukal, and D. A. Vossler, Crustal refraction profile, Oregon coast range, *Bull. Seismol. Soc. Amer., 56,* 1357–1362, 1966.

Bonini, W. E., D. W. Hughes, and Z. F. Daneš, Complete Bouguer gravity anomaly map of Washington, *Geol. Map GM-11,* State of Wash. Dep. of Natur. Resour., Seattle, 1974.

Burdick, L. J., and D. V. Helmberger, Time functions appropriate for deep earthquakes, *Bull. Seismol. Soc. Amer., 64,* 1419–1428, 1974.

Burdick, L. J., and D. V. Helmberger, The upper mantle *P* velocity structure of the western United States, *J. Geophys. Res., 83,* 1689–1712, 1978.

Burdick, L. J., and C. A. Langston, Modeling crustal structure through the use of converted phases in teleseismic body-wave forms, *Bull. Seismol. Soc. Amer., 67,* 677–691, 1977.

Daneš, Z. F., M. M. Bonno, E. Brau, W. D. Gilham, T. F. Hoffman, D. Johansen, M. H. Jones, B. Malfait, J. Masten, and G. O. Teague, Geophysical investigation of the southern Puget Sound area, Washington, *J. Geophys. Res., 70,* 5573–5580, 1965.

Dehlinger, P., E. F. Chiburis, and M. M. Colver, Local travel-time curves and their geologic implications for the Pacific Northwest states, *Bull. Seismol. Soc. Amer., 55,* 587–607, 1965.

Dey-Sarkar, S. K., and R. A. Wiggins, Upper mantle structure in western Canada, *J. Geophys. Res., 81,* 3619–3632, 1976*a*.

Dey-Sarkar, S. K., and R. A. Wiggins, Source deconvolution of teleseismic *P* wave arrivals between 14° and 40°, *J. Geophys. Res., 81,* 3633–3641, 1976*b*.

Fiske, R. S., C. A. Hopson, and A. C. Waters, Geology of Mount Rainier National Park, Washington, *U.S. Geol. Surv. Prof. Pap., 444,* 93 pp., 1963.

Hagiwara, T., A note on the theory of the electromagnetic seismograph, *Bull. Earthquake Res. Inst. Tokyo Univ., 36,* 139–164, 1958.

Haskell, N. A., Crustal reflection of plane *SH* waves, *J. Geophys. Res., 65,* 4147–4150, 1960.

Haskell, N. A., Crustal reflection of plane *P* and *SV* waves, *J. Geophys. Res., 67,* 4751–4767, 1962.

Havskov, J., and E. R. Kanasewich, Determination of the dip and strike of the Moho from array analysis, *Bull. Seismol. Soc. Amer., 68,* 1415–1419, 1978.

Helmberger, D., and R. A. Wiggins, Upper mantle structure of midwestern United States, *J. Geophys. Res., 76,* 3229–3245, 1971.

Hong, T.-L., and D. V. Helmberger, Glorified optics and wave propagation in nonplanar structure, *Bull. Seismol. Soc. Amer., 68,* 1313–1330, 1978.

Johnson, S. H., and R. W. Couch, Crustal structure in the North Cascade Mountains of Washington and British Columbia from seismic refraction measurements, *Bull. Seismol. Soc. Amer., 60,* 1259–1269, 1970.

Jordan, T. H., and L. N. Frazer, Crustal and upper mantle structure from *Sp* phases, *J. Geophys. Res., 80,* 1504–1518, 1975.

Keith, C. M., and S. Crampin, Seismic body waves in anisotropic media: Synthetic seismograms, *Geophys. J. Roy. Astron. Soc., 49,* 225–243, 1977.

Key, F. A., Signal-generated noise recorded at the Eskdalemuir seismometer array station, *Bull. Seismol. Soc. Amer., 57,* 27–37, 1967.
Kurita, T., A procedure for elucidating fine structure of the crust and upper mantle from seismological data, *Bull. Seismol. Soc. Amer., 63,* 189–209, 1973.
LaFehr, T. R., Gravity, isostasy, and crustal structure in the Southern Cascade Range, *J. Geophys. Res., 70,* 5581–5597, 1965.
Langston, C. A., Corvallis, Oregon, crustal and upper mantle receiver structure from teleseismic *P* and *S* waves, *Bull. Seismol. Soc. Amer., 67,* 713–724, 1977*a*.
Langston, C. A., The effect of planar dipping structure on source and receiver responses for constant ray parameter, *Bull. Seismol. Soc. Amer., 67,* 1029–1050, 1977*b*.
Langston, C. A., and D. E. Blum, The April 29, 1965, Puget Sound earthquake and the crustal and upper mantle structure of western Washington, *Bull. Seismol. Soc. Amer., 67,* 693–711, 1977.
Lin, J. W., A study of upper mantle structure in the Pacific Northwest using *P* waves from teleseisms, Ph.D. thesis, 98 pp., Univ. of Wash., Seattle, 1974.
McKenzie, D., and B. Julian, Puget Sound, Washington, earthquake and the mantle structure beneath the northwestern United States, *Geol. Soc. Amer. Bull., 82,* 3519–3524, 1971.
Mitchell, B. J., and M. Landisman, Electromagnetic seismograph constants by least-squares inversion, *Bull. Seismol. Soc. Amer., 59,* 1335–1348, 1969.
Riddihough, R. P., The Juan De Fuca plate, *Eos Trans. AGU, 59,* 836–842, 1978.
Sacks, I. S., and J. A. Snoke, The use of converted phases to infer the depth of the lithosphere-asthenosphere boundary beneath South America, *J. Geophys. Res., 82,* 2011–2017, 1977.
Sengupta, M. K., and B. R. Julian, *P*-wave travel times from deep earthquakes, *Bull. Seismol. Soc. Amer., 66,* 1555–1579, 1976.
Smithson, S. B., Modeling continental crust: Structural and chemical constraints, *Geophys. Res., Lett., 5,* 749–752, 1978.
Snavely, P. D., and H. C. Wagner, Tertiary geologic history of western Oregon and Washington, *Invest. 22,* 25 pp., Div. of Mines and Geol., Olympia, Wash., 1963.
Snoke, J. A., I. S. Sacks, and H. Okada, Determination of the subducting lithosphere boundary by use of converted phases, *Bull. Seismol. Soc. Amer., 67,* 1051–1060, 1977.
Unger, J. D., and R. W. Decker, The microearthquake activity of Mt. Rainier, Washington, *Bull. Seismol. Soc. Amer., 60,* 2023–2035, 1970.
Unger, J. D., and K. F. Mills, Microearthquakes at Mt. Rainier—1969, *Bull. Seismol. Soc. Amer., 62,* 1079–1081, 1972.
Zuercher, H., A study of the crust in Puget Sound using a fixed seismic source, M.S. thesis, 62 pp., Univ. of Wash., Seattle, 1975.

(Received December 27, 1978;
revised February 23, 1979;
accepted February 26, 1979.)